Teaser By explicitly representing ocular anatomy, computational fluid dynamic simulation methods model drug mass transport both within and between ocular tissue regions, providing reliable animal-to-human translation of bioavailability.Here, we apply physiologically based models to simulate ocular drug administration. A non-anatomical model is used that applies a simple theorem for calculating ocular bioavailability from a topical dose. A computational fluid dynamic model is also described that incorporates ocular physiology in anatomical models for rabbit, monkey and man. This second method applies material properties and boundary conditions for various tissues enabling simulation of fluid flows, pressures, temperatures, convection, and drug advection following various modes of administration. The method provides a regional distribution with a given tissue not available using standard compartmental models, and enables translation of results from animal experiments into predictions for human ocular pharmacokinetics (PK).

Physiologically based ocular

Paul J. Missel and Ramesh Sarangapani

Data Science and Digital Solutions, Alcon Vision LLC, Fort Worth, TX, USA

Introduction

Ocular PK is the science behind the kinetics of drug distribution throughout, and its elimination from, ocular tissue. Ocular pharmacodynamics (PD) is the science quantifying drug effects mediated through pharmacokinetics. Here, we focus on describing various PK modeling approaches and illustrate how they are put to effective use in the design of advanced ocular therapeutics.

Ophthalmic drugs elicit their pharmacological effects on specific tissues. In the case of ocular allergy, the target tissue is immediately accessible on the ocular surface, and is treatable with topical dosing. Tissue targets internal to the eye but located near the anterior are accessible using topical administration, but tear turnover and conjunctival vascular clearance reduce the concentration, requiring frequent dosing. Depending upon the properties of the drug, ocular fluid flow patterns and vascular clearance can provide either additional hindrances against or opportunities for accessing tissue targets deep within the ocular interior using topical administration.

Self-administered topical doses are difficult to perform, and the requirement for frequent dosing imposes a treatment burden and a problem with noncompliance, which work against effective therapy. Devices and dosage forms provide a platform for sustained delivery of drug that offers to remove this burden and to circumvent noncompliance. However, their effective design requires an understanding of the physiological processes at work within the eye. These processes must be considered when developing models to aid in the design of ophthalmic pharmaceuticals.

There are different types of numerical modeling method that have been applied to the eye. Noncompartmental methods attempt to characterize drug exposure without using detailed models, focusing entirely upon describing the data. Classical compartmental PK modeling, as the name implies, approximates the ocular system as a series of compartments representing key target tissues within the eye. Dose is administered at a prespecified location in the model and the drug PK is estimated typically assuming first-order transfer of material between compartments. The number of compartments to describe the ocular system in a compartmental PK model is typically derived empirically and might not relate to the physiology and/or anatomy of the actual biological system. Physiologically based PK (PBPK) models attempt to improve upon classical models by associating compartments with specific tissues and to incorporate aspects of anatomy in how the compartments are interlinked. Furthermore, PBPK models use observed physiological processes, such as fluid flow rates, as a basis to quantify intercompartmental exchange. An example of a PBPK ocular model for the disposition of pilocarpine after topical dosing appears in Fig. 4 of [1]. Commercial software is available that uses the compartmental approach, with information built into the system to represent the ocular behavior for various drug classes [2].

Paul Missel is Therapeutic Area Modeler at Alcon. For more than thirty years, he has modeled diverse aspects of ocular therapeutics including drug delivery, medical devices and surgical procedures for cataract, vitrectomy, and corneal refractive correction. Modeling techniques have ranged from simple mathematical descriptions to multiphysics simulations of fluid flow, mass transport, and mechanical response using high performance computing. Other areas of focus have included analytical chemistry, spectroscopy, and dissolution science applied to ocular pharmaceuticals. He has authored or co-authored more than 70 publications, presentations and patents. He received SB and PhD degrees in Physics from MIT.

Ramesh Sarangapani is Head of Data Science Digital Health at Alcon, a Novartis Company. He has more than 20 years' experience managing project teams and in applying advanced analytics for product development in the pharmaceutical and medical device industry. In his current role he oversees the application of machine learning and digital technology to drive product innovation and commercialization. Dr. Sarangapani received his BTech in Mechanical Engineering from the Indian Institute of Technology, Chennai, and his PhD in Bioengineering from the University of Delaware.

Corresponding author: Missel, P.J. (paul.missel@alcon.com)

https://doi.org/10.1016/j.drudis.2019.05.039

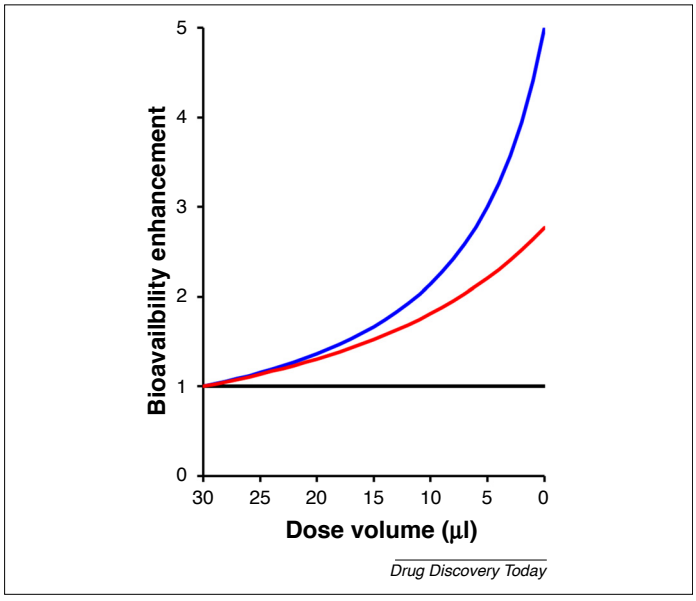

FIGURE 1

Potential increase in bioavailability that would result from reducing the volume of a simple drug solution administered as a topical dose, compared to a 30 µl dose. Based on the analysis by Keister *et al.* [9].

Mixed-effects modeling, which is also called population-based modeling, is a methodology developed to account for both variability in biological systems and inherent stochasticity or randomness in both the stimuli and response typical to biological systems. Mixed-effects modeling approach can be applied to either classical PK compartmental models or PBPK models. However, the approach is often focused on characterizing population trends through covariates (such as race, gender, etc.), which is enabled by modeling both the typical population behavior and the between-subject variability [3].

One PK modeling approach uses finite-element or finite-volume methods applied to engineering models, which accurately represent ocular anatomy and physiology. Computer-aided design (CAD) software has been used to construct anatomically accurate models for human, monkey, and rabbit eyes [4]. This modeling procedure can be considered as an extension of PBPK compartmental modeling, because the explicit geometric models can associate compartments with particular tissues. Fluidic processes within a compartment can be simulated, using tissue properties and boundary conditions as appropriate, to replicate physiological flows. Modeling these flows can replicate physiological processes of cell depositions (Krukenberg's spindle) that have been imputed to such flows [5,6]. Geometric models can even accommodate motion of tissues, for example, the motion of the iris during visual accommodation and blinking [7,8].

The focus of our current discussion is to develop these simulation methods so that they can determine the time course of drug disposition from any mode of administration. We begin with an examination of topical ocular drug treatment, applying physiology to analytical mathematical derivations for a non-anatomical model of the decay of drug concentration in the tear film after instillation of a topical dose. We then progress to an approach that incorporates the anatomy and physiology of the eye, the ocular computational fluid dynamic (CFD) model. This model is applied to simulating the time distribution of drug within the internal ocular space following topical dosing and intravitreal injection. Simulations are conducted in model eyes for various species (rabbit, monkey, and human) to demonstrate the degree of model qualification for available literature data and to illustrate how the approach will enable scaling of results from animal experiments to ocular PK in the human eye.

Non-anatomical physiological modeling example: topical dosing

Before the availability of advanced multiphysics software, various general mathematical approaches were used to model topical dosing. In topical dosing, several factors interfere with the delivery of drug into the ocular interior. There is a practical limit to the volume of a liquid medication that can be accommodated in the precorneal area without spilling out. Moreover, the rate of drainage increases with increasing dose volume. Not all drug in the precorneal space gets absorbed into the cornea, some is absorbed into the conjunctiva and is cleared by the conjunctival vasculature. Keister *et al.* [9] cite several experimental studies measuring the influence of dose volume on ocular bioavailability, and present a mathematical analysis predicting how ocular bioavailability depends on dose volume accounting for these affects. A few key results are presented here.

A useful theorem [9] states that the total ocular bioavailability (OB) through the cornea from a topical dose is given by Equation 1:

$$OB = A_c k_{per} \int_0^\infty C_T(t)\, dt \qquad [1]$$

where A_c is the corneal surface area, k_{per} is the corneal permeability coefficient, and $C_T(t)$ is the time-dependent concentration in the tear film. In this simple theorem, the geometric model of the eye is reduced to an undefined geometric domain on one side of a membrane surface; here, we are only concerned about what can be done to increase the amount of drug that will be delivered across the corneal surface by altering the topical dose formulation.

We begin by considering only simple aqueous solutions of a drug. The constraints of the packaging determine that the doses administered will have a particular volume. The volume of the dose will have an important influence on the bioavailability, because the rate at which the tear fluid reservoir drains away increases with the dose volume [10]. The larger the dose volume, the greater the nonproductive loss of drug from tear drainage will be because the time integral of $C_T(t)$ will be reduced. This nonproductive loss can be lowered by reducing the dose volume. The magnitude of loss reduction is dependent upon the magnitude of k_{per}. If drug permeability is slow (low k_{per}), bioavailability loss through drainage of excess precorneal fluid volume can be effectively decreased by reducing dose volume (at constant amount of drug dosed). As permeability increases, the benefit of this strategy is reduced, because the drug has a greater opportunity to diffuse into the cornea before it is lost through drainage.

Figure 1 shows how the bioavailability of a topical dose of timolol would benefit by reducing the dose volume from 30 µl to zero while keeping the total amount of drug dosed constant. (Here, we ignore the potential impracticality of being able to administer small dose volumes, the discomfort that might result

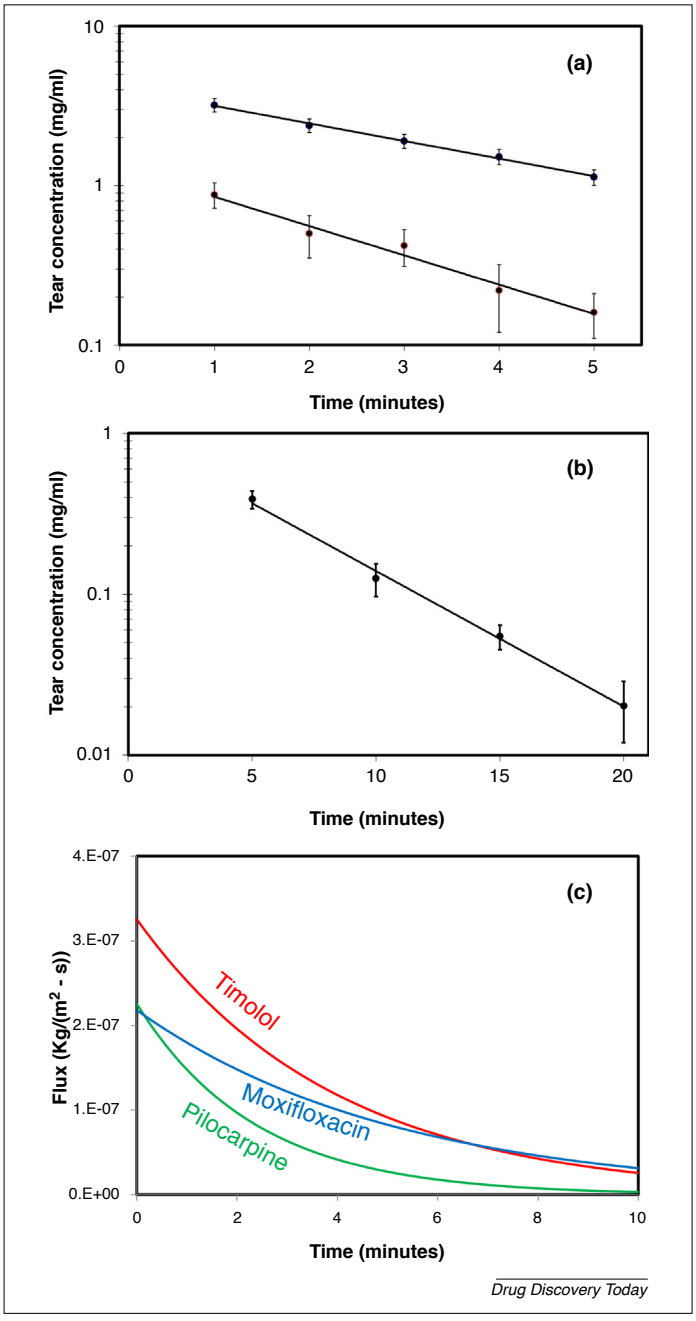

FIGURE 2

Experimentally measured tear film concentrations and imputed precorneal fluxes for three drugs following topical dosing. (a) Upper curve: 25 μl dose of 0.65% timolol maleate; data from [11]. Lower curve: 25 μl dose of 0.27% pilocarpine nitrate; data from [1]. (b) 45 μl of 0.3% moxifloxacin hydrochloride. Following dosing, manual blinking was performed at the rate of 4 blinks/min and BSS PLUS® irrigating solution was added at the rate of 2 μl/min; data from [30]. (c) Flux of drug through cornea, product of k_{per} × tear film concentration, before multiplying by the amplitude factor, which accounts for nonproductive losses by absorption through precorneal tissues.

from instilling highly concentrated solutions, and the implications of dispensing undissolved drug powder in the limit of zero volume.) The curve for timolol was calculated using the asymptotic expression derived in the appendix of [9], assuming an undisturbed tear reservoir volume of 7.5 μl and a value of 7.98 × 10^{-6} cm/s for the corneal permeability coefficient as measured by Ahmed *et al.* [11]. The curve shows a potential increase in bioavailability of between two- to threefold as the dose volume is reduced to zero, and is about halfway between two curves, which shows the enhancements projected in the limit of very slow, and very rapid corneal permeability. In the limit of infinitely rapid permeability, there would be no benefit from reducing dose volume and, thus, the limiting behavior in this case is the horizontal line (bioavailability is independent of dose volume at constant amount dosed). In the limit of very low permeability, the bioavailability scales with the ratio of the undisturbed resident tear volume V_0 divided by the total post-instillation tear volume (Eqution 2):

$$\int_0^\infty C_T(t)dt \sim \left(\frac{V_0}{V_0 + V_d}\right) \quad [2]$$

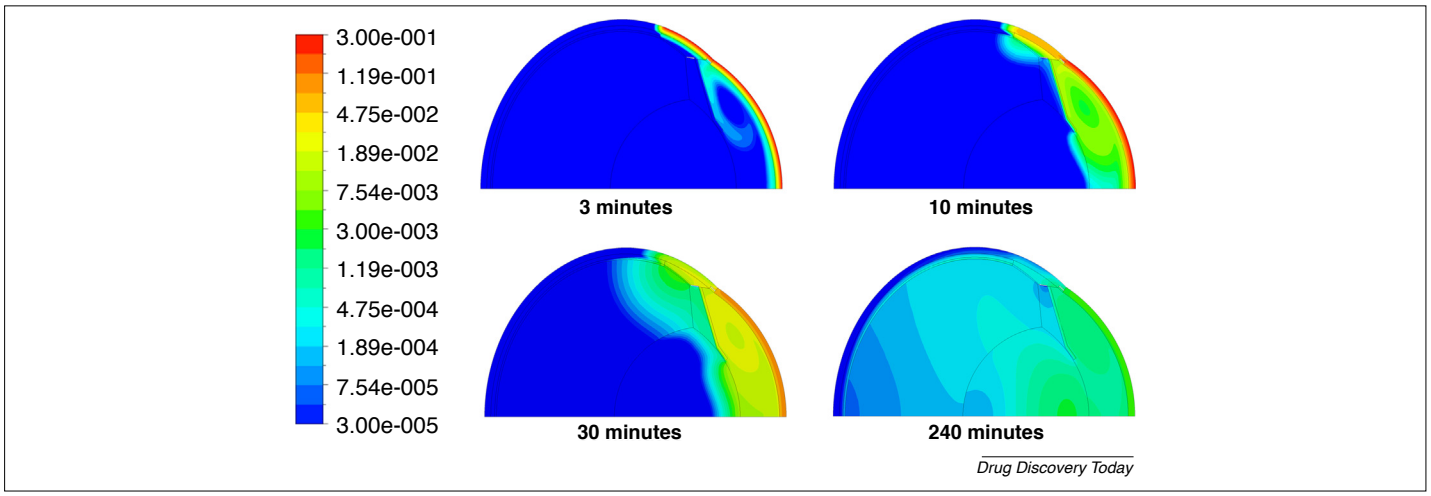

FIGURE 3

Simulated advection of drug into ocular tissue following topical dosing with moxifloxacin. Time after dosing is indicated below each figure.

where V_d is the volume of the dose administered. Using a value of 7.5 μl for V_0, the value of the integral increases fivefold when V_d is reduced to zero.

Although there are several innovative approaches that have been developed for administering topical ophthalmic doses with reduced volume, we are not aware of any clinical data using this approach for increasing the bioavailability for timolol. However, two separate strategies demonstrated a twofold enhancement in the bioavailability of this drug. One strategy used by TIMPOTIC-XE is to incorporate a biopolymer that spontaneously forms a gel when mixed with tear fluid. Nonproductive losses from tear drainage of excess precorneal fluid are not minimized by reducing dose volume but rather by the formation of a gel, which essentially eliminates the rapid initial loss of excess precorneal fluid volume. The benefit demonstrated from this approach is a twofold enhancement in bioavailability, comparable to the benefit predicted for timolol in Fig. 1 .

A second formulation strategy is the inclusion of sorbic acid in the formulation. Sorbic acid forms an ion pair with timolol, increasing its lipophilicity and, thus, also increasing the bioavailability of topically administered timolol by approximately twofold [12]. It is not anticipated that sorbic acid would alter the drainage kinetics of a topically administered dose. This increase in bioavailability arises from a completely different mechanism; it is the result of a twofold increase in the chemical partitioning of timolol into the corneal epithelial tissue. In developing physiologically based PK models, it is important to include tissue partitioning effects, as discussed later.

Anatomical physiological modeling approach: the ocular CFD model

A comprehensive model for ocular drug disposition should incorporate several physiological processes, such as: production and elimination of tears; production, elimination, and thermal convection of aqueous humor; chemical partitioning between tissue compartments; diffusion within each tissue compartment; hydraulic flow through tissues considered as porous media; hydraulic efflux through exterior tissue boundaries; elimination by vascular flow (conjunctiva, iris, ciliary body, and choroid); elimination from the lymphatic system; fluid currents produced in partially liquefied vitreous regions from ocular motion; temporary fluid currents arising from transient pressure rise following injection; binding of drug to ocular components and melanin binding; and metabolism and active transport.

Compartmental physiologically based models attempt to incorporate some of the effects above in an approximate manner, imputing the effects of fluid production and/or elimination and vascular clearance through judicious assignments of intercompartment transfer coefficients. Information from the anatomy and physiology is incorporated in an approximate manner. Beginning during the 1990s, investigators applied finite element software to simulate diffusion of drug in geometric models for the eye [13–28]. The development of various finite element modeling approaches for the eye are reviewed briefly in Ref. [29].

Finite element modeling typically begins with an *in silico* construction of a geometrically accurate model of the domain to be simulated. Various regions are assigned physically meaningful material properties, and boundary conditions are imposed to enable the imposition of fluid flow, pressure, and temperature constraints as appropriate. The software uses this information as input for the solution of equations describing the transport of fluid and drug by processes of diffusion and convection. An example for the problem setup for modeling drug disposition in the rabbit eye is described in detail in Ref. [4]. As such, this approach can be considered as an extension of PBPK compartmental modeling, because the explicit geometric models can associate compartments with particular tissues.

Ocular CFD model application: topical dosing

To illustrate the ocular CFD modeling method, we apply it to modeling the intraocular disposition of drug following topical dosing for three drugs. The model used for this purpose does not articulate the anatomy of the ocular adnexa, such as the lids, tear glands, tear ducts, and tear reservoir, but contains tissues only within the globe itself (refer to Fig. 4 of [4]). Instead of attempting to explicitly model the mixing of drug solution with tear fluid, the dilution from produced tears, the dynamics of blinking and absorption into the eyelid tissue, the clearance from the conjunctival

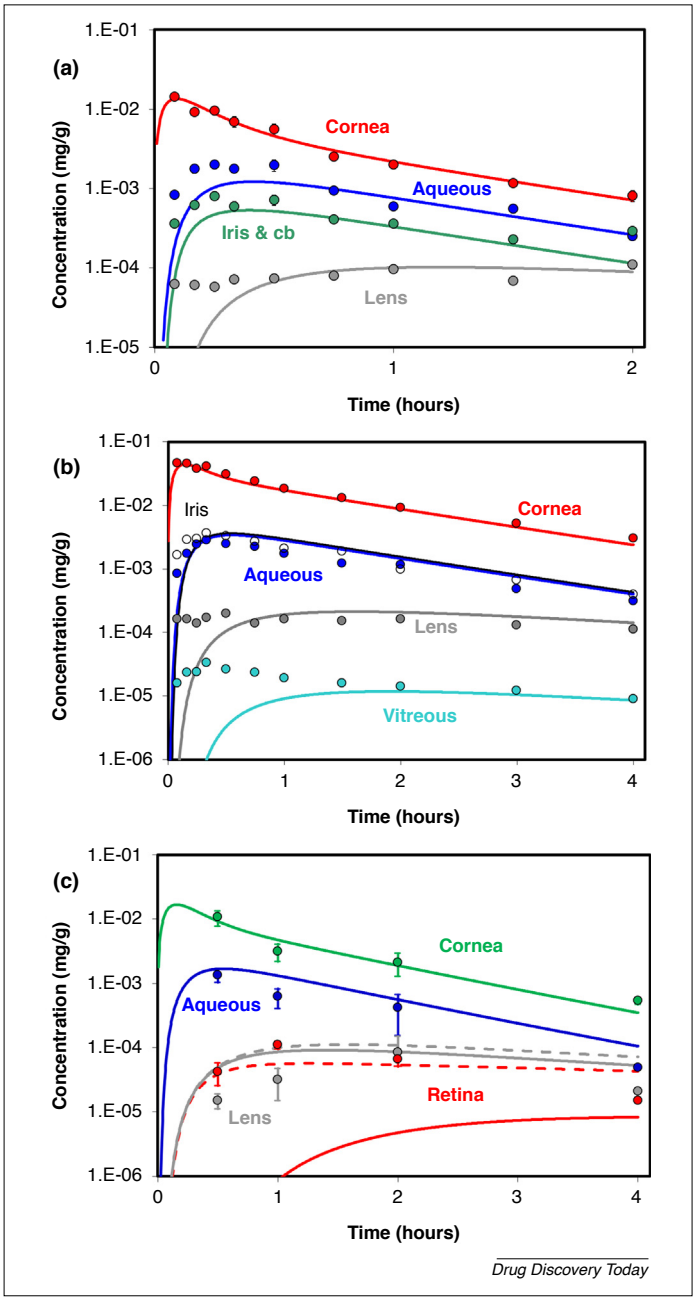

FIGURE 4

Comparison between simulated and experimental mean tissue compartment concentrations following topical dosing. **(a)** 25 μl dose of 0.27% pilocarpine nitrate; data from [1]. **(b)** 25 μl dose of 0.65% timolol maleate; data from [33]. **(c)** 30 μl dose of 0.3% moxifloxacin hydrochloride; data from an Alcon study previous to [32]. The solid curves in all three panels show simulations in which the transient flux profiles for each drug taken from Fig. 2 c are applied to the outer corneal surface. The broken curves in (c) show simulations of the flux profile for moxifloxacin applied to both the outer corneal and the outer anterior scleral surface. Reproduced from [34] (b).

circulation, and so on, we impute a time-dependent flux of drug through the anterior corneal surface from the experimentally measured drug concentrations in the tear film following topical dosing, as shown in Fig. 2 .

For each of the drugs studied (pilocarpine [1,10,30], moxifloxacin [31,32], and timolol [11,12,33]), the tear film concentration decays exponentially. We input drug into our ocular model with the transient first-order flux conditions as shown in Fig. 2 c, using the relationship flux = Amplitude × k_{per} × concentration, where k_{per} is the corneal permeability coefficient (see Table 1a for coefficients derived for the first-order drug input functions and experimentally determined values of k_{per} for each drug). Amplitude (Table 1d) is a prefactor that is empirically derived from a fit to the data and that accounts for nonproductive losses of drug during administration. We then allow the drug to permeate throughout the ocular tissue and to be distributed by diffusion and convection. At boundaries separating ocular tissues having different properties, there will be a discontinuity in drug concentration reflecting the ratio of the chemical partition coefficient for drug in each tissue. Table 1b shows the partition coefficients used in the simulations, which were taken approximately from the experimental measurements of Miller *et al.* [1] for pilocarpine and of Francoeur *et al.* [33]

TABLE 1

Model parameters used in simulating ocular bioavailability from topical dosing

	Drug		
	Pilocarpine nitrate	**Timolol maleate**	**Moxifloxacin HCl**
(a) Coefficients used to generate flux boundary condition for simulating topical dosing			
$C_{t,0}$ (μg/ml)	1300[a]	4084[a]	2400[b]
k_t (min^{-1})	0.423[a]	0.254[a]	0.194[a]
k_{per} ($cm\ s^{-1}$)	1.74×10^{-5}[c]	7.98×10^{-6}[d]	9.1×10^{-6}[e]
(b) Partition coefficients for albino ophthalmic tissues used in topical dose simulations			
Aqueous, vitreous	1[f]	1[g]	1[g]
Cornea	1.81[f]	4[g]	2.2 [g]
Choroid, retina, sclera, TM	1[f]	2.2[g]	2.2[g]
Ciliary body, iris	2[f]	2.2[g]	2.2[g]
Lens	1[f]	0.94[g]	0.94[g]
(c) Diffusion coefficients for ophthalmic tissues used in topical dose simulations ($cm^2\ s^{-1}$)			
Aqueous, vitreous	9.74×10^{-6}	8.34×10^{-6}	8.34×10^{-6}
Cornea, sclera, TM	7.31×10^{-7}	6.26×10^{-7}	6.26×10^{-7}
Choroid, retina	7.31×10^{-8}	6.26×10^{-8}	6.26×10^{-8}
Ciliary body	7.31×10^{-7}	1.07×10^{-7}	6.26×10^{-7}
Iris	7.31×10^{-7}	1.07×10^{-7}	1.07×10^{-7}
Lens	7.31×10^{-7}	1.31×10^{-6}	1.31×10^{-6}
(d) Additional parameter values used in simulations of topical dosing			
Iris sink strength (s^{-1})	3×10^{-3}	2×10^{-3}	3×10^{-3}
Choroid sink strength (s^{-1})	1	1	1×10^{-4}
Amplitude	0.175	0.25	0.12

[a] Value obtained from the fit to the data in Fig. 2 a (main text).
[b] Value adjusted to provide an initial tear concentration assuming perfect mixing of a 30 μl dose with 7.5 μl resident tears.
[c] From [31].
[d] From [11].
[e] From [32].
[f] From [1].
[g] Approximately based on values measured for timolol from [33] (see main text).

for timolol. The partition coefficients measured for timolol were also used for moxifloxacin. The value of the partition coefficient for timolol in the cornea was adjusted from 2.2 to 4 to allow for a better fit.

Table 1c shows the diffusivities used for each tissue region for each drug. The values of diffusivity in the aqueous humor were anchored to the value of diffusivity quoted for timolol in aqueous solution from Ahmed *et al.* [11], and adjusted upward by the cube root of the ratio of molecular weights for pilocarpine. The values for timolol were used for moxifloxacin, which has a molecular weight comparable to that of timolol. Values for other tissues were reduced to reflect the values as determined from the tissue transport measurements for anecortave acetate, another lipophilic drug for which such data are available [27].

As drug is transported through vascularized regions of the ocular tissue, a portion of the drug is removed. The efficiency of removal is dependent upon the molecular properties of the drug. Therefore, we tune the strength of the vascular sink applied in these regions so that the model can reproduce the rate of ocular drug clearance. Table 1d lists the values of the vascular sink strengths applied in the regions of the iris and the choroid. A sink of identical strength to that applied in the choroid was also applied in the retina and the ciliary body. Also appearing in Table 1d is the amplitude prefactor multiplying the $k_{per} \times$ concentration versus time profiles for the drug input function. The amplitude is <1 because without explicitly including the exterior anatomy in our model, there is no ability to simulate losses to the ocular adnexa.

The simulation of the fluidic flow patterns within the eye have been discussed in detail previously [4,29]. The aqueous humor is treated as a simple fluid with the properties of water; all other tissues are treated as porous media with the hydraulic resistivities specified in Table 2a. Regional differences in temperature give rise to thermal convection within the aqueous humor compartment. The pressure and flow solutions are shown in Fig. 2 of [34] (see also Figs 2 and 3 of [28]). In these simulations, the corneal temperature was maintained at 34 °C, the retina, choroid, sclera, iris, and ciliary body were maintained at 37 °C, and the temperature in the vitreous, lens and aqueous humor, was not constrained. The Boussinesq approximation, in which the effect of temperature on the fluid density is accounted for in the momentum equations, enables the simulation of thermal convection within the aqueous compartment [5,6]. The parameters used in the current model are detailed in Table 2b.

The additional specification required is the magnitude and direction of the gravitational force, which was applied along the symmetry axis (eye looking upward). By using an axisymmetric model for the eye, it is not possible to model the eye looking horizontally. A 3D model would be required, and this will impact the flow pattern [6]. In either orientation, thermal convection renders the aqueous humor compartment to be a well-stirred chamber. The fluid flow pattern in the aqueous compartment for the current model is illustrated in Fig. 2 c of [4]. There is also a minute flow of fluid through the porous vitreous gel, as illustrated in Figure 12 of [4]. The physics of the flow is governed by a

TABLE 2

Model parameters used in simulating drug disposition following intravitreal injection

(a) Hydraulic resistivity values assigned to various tissue regions	
Tissue	Hydraulic resistivity (m^{-2})
Vitreous	1.725×10^{13}
TM[a]	8.76×10^{15}
All other tissues except aqueous humor	9.66×10^{17}

(b) Properties of the aqueous humor used for the Boussinesq approximation	
Property	Value
Density (kg/m^3)	991.27
Specific heat ($J/kg-^{\circ K}$)	4200
Thermal conductivity ($W/M-^{\circ K}$)	0.6
Viscosity (kg/M^{-s})	6.9×10^{-4}
Thermal expansion ($1/^{\circ}K$)	3×10^{-4}

Tissue	Avastin	Lucentis
(c) Diffusion coefficients for ophthalmic tissues ($cm^2\ s^{-1}$)		
Aqueous, vitreous[b]	5.21×10^{-7}	7.82×10^{-7}
Cornea, sclera, TM, ciliary body, iris	3.91×10^{-8}	5.86×10^{-8}
Choroid, retina	3.91×10^{-9}	5.86×10^{-9}
Lens	$2.61 \times x\ 10^{-8}$	3.91×10^{-8}
(d) Values of regional sinks (s^{-1})		
Choroid	2.5×10^{-5}	2.5×10^{-5}
Ciliary body	6.25×10^{-6}	6.25×10^{-6}

[a] Adjusted to achieve a desired hydraulic pressure. The values in this table are consistent with a viscosity value of 6.9×10^{-4} kg/m^{-s} for the viscosity of percolating fluid, the value for water at 37 °C.

[b] Used values determined from dynamic light-scattering measurements from [56], adjusted for temperature.

different set of equations. In the aqueous humor, the Navier–Stokes equations are modeled, whereas the flow in all the other tissue compartments follows the Darcy law, where flow follows the gradient in pressure. The maximum velocity for the hydraulic flow in the vitreous is four orders of magnitude slower than the maximum velocity within the aqueous humor.

Figure 3 shows simulations of the drug distribution within ocular tissue following topical dosing with moxifloxacin. Note that a logarithmic color scale is used for drug concentration. The transient flux profile from Fig. 2 c was applied to the outer corneal and anterior scleral surfaces. At 3 min, a small amount of drug had traversed the cornea and begun mixing in the well-stirred aqueous chamber. At 10 min, drug had permeated throughout the ciliary body, and was beginning to enter the anterior lens and vitreous compartments. As time proceeded, the concentration in the anterior compartments at first increased with time, but then decreased as drug concentration was reduced by aqueous humor turnover and as it distributed throughout the vitreous. A small concentration of drug reached the retina rather quickly after diffusing through the ciliary body, rather than diffusing from the aqueous humor into the vitreous, and that drug slowly accumulated in the lens. The effect of vascular clearance in the ciliary body is apparent as the color contours change with time. Were these simulations to be carried out for longer, it would be apparent that the lens is acting as a depot, slowly releasing the drug that it took in at an early time when the local concentration adjacent to the anterior lens surface was high.

Figure 4 compares simulations of the mean tissue compartment concentrations with experimental measurements following topical dosing. Simulations were conducted using the properties for each drug as specified in Table 1. The simulations do a fair job of predicting the concentrations for the anterior most compartments, but the simulated concentrations in the vitreous and lens for pilocarpine and timolol lag behind the experimental values. Drug appears in the vitreous and lens more quickly than is explained by the model. The predictions for the lens compartment concentrations for moxifloxacin fare better than the other drugs, but the simulation for the retinal compartment lags in time. If the flux condition is also extended to the outer surface of the anterior sclera, drug appears in the retina more quickly (broken curves in Fig. 4 C).

The data suggest that drug is distributed among interior ocular tissue compartments more rapidly than is predicted by diffusion and advection in the simulated flow field, which suggests that there are additional internal ocular fluid currents or vascular recirculation pathways capable of transporting drug from one tissue compartment to another. The model could be improved by incorporating these fluidic and circulatory currents, provided the incorporations accurately reflect ocular physiology.

Ocular CFD model application: IVT injection

Topical dosing will not provide adequate delivery of most drugs intended to treat tissues deep within the eye, such as the retina. The standard of care for treatment of age-related macular degeneration (AMD) is the injection of a protein, such as Lucentis, directly into the vitreous. In modeling the disposition of drug following intravitreal (IVT) injection, the initial condition is frequently assumed to be a perfectly spherical bolus of drug centered around the needle orifice. In reality, the process of IVT injection is complex, given that it involves the injection of one fluid into another with very different properties [35,36]. Moreover, the intraocular pressure is elevated because the tissues of the outer sheath are elastic [37]. Once the needle is withdrawn, a portion of the injected material might flow away from the region of injection by following along the path of the needle [38]. Some of it might be expelled through the needle hole, but a portion might be drawn into the various layers between the tissues in the outer sheath, or the layers between the retina and choroid or the choroid and sclera. If the site of injection is toward the anterior, it is possible that a portion of the bolus might be expelled immediately into the aqueous humor. If it is near the outer tissues, then the excess pressure close to the needle opening might be sufficient to drive several percent of the injected bolus directly into the retina, choroid, and sclera (see Fig. 4 .4 of [29]).

Thus, before the first experimental time point occurs, even if it is only a few minutes after injection, it has been our experience that only a fraction (typically 4–80%) of the total injected drug is recovered from all tissues. Drug that is in intimate contact with the exterior tissues can be cleared quickly by the choroidal vasculature even if it is not expelled out through the needle hole left behind in the sclera. The initial portion of the injection that remains in the vitreous has an irregular shape [39]. The injected fluid does not necessarily mix immediately with the vitreous but can move to another location under the influence of gravity [40].

Another factor that adds to the complexity is the variability of the rheological properties of the vitreous fluid among various animal species and changes in the vitreous that occur upon aging

[41–43]. These differences in vitreous rheology will likely cause variability in the initial distribution and possibly also the rate of clearance after IVT injection or device implantation. The clearance of IVT-injected triamcinolone acetonide suspension in one patient who had undergone vitrectomy was faster than for other patients who had not undergone vitrectomy [44]. The clearance of IVT-injected VEGF was faster in rabbits that had undergone vitrectomy than in rabbits that had not undergone vitrectomy [45]. However, the delivery profile of dexamethasone from an IVT implant was unaffected by vitrectomy [46].

Although all of the complications of IVT injection are worthy of separate investigation, eventually the drug diffuses away from its irregular shape and establishes a quasi steady-state distribution in drug concentration that decays steadily with time under the influences of the physiological flows and vascular sinks. Thus, simulations in which the initial condition for the bolus is a simple sphere located in a particular region of the vitreous might not capture all of the intricacies of a particular injection site or modality; they are perfectly acceptable as a starting point for determining the clearance behavior after the quasi steady-state distribution is established.

Before drug can become cleared from the vitreous, it first has to diffuse or convect from the site of the bolus until it fills the entire compartment. This is referred to as the 'distribution' phase. Eventually concentration gradients will be established, with the lowest concentrations adjacent to the tissue boundaries where the clearance of drug is most effective. The pattern of concentration gradients, once established, will tend to remain constant in a geometric pattern, whereas the concentration at every point within the vitreous decreases exponentially; this is referred to as the 'elimination' phase.

The concentration gradients established in the elimination phase for two different types of molecule are shown in Fig. 5 . Fluorescein is effectively cleared through the retina and choroid by a transport mechanism; thus, the lowest concentrations are adjacent to the retina (Fig. 5 a [47,48]). The highest concentration within the vitreous occurs behind the lens, which is avascular. When the dominant means of clearance occurs through the retina and/or choroid, this type of clearance is referred to as the 'posterior pathway'. The concentration profile observed for a hydrophilic dextran polymer (Fig. 5 b) is different. In this case, the highest concentration occurs at the back of the vitreous, and the most effective means of clearance is by diffusion through the hyaloid membrane, after which the portion that diffuses across the hyaloid membrane is mixed efficiently with the aqueous humor and is eliminated through the canal of Schlemm. This route of clearance is referred to as the 'anterior pathway'. The data for sucrose [49] and albumin [50] also seem to be cleared by the anterior pathway. The anterior pathway is always engaged; note that there is a gradient with a lower concentration towards the anterior along the lens boundary in Fig. 5 a.

Figure 5 c,d show concentration profiles simulated using only the aqueous and vitreous compartments of the ocular CFD model for the rabbit. In both of these simulations, the initial condition was a spherical bolus placed in the mid-vitreous. The diffusivity was assigned to match the diffusivity in buffer at physiological temperature for each molecule. The rate of fluid entering the inlet (on the ciliary body just behind the iris) was 3 μl/min. The simulation for dextran shown in Fig. 5 d did not impose any drug sink on the outer vitreous boundary; the only mechanism for drug elimination is by diffusion into the aqueous humor and outflow through the pressure outlet [which was located at the surface of the trabecular meshwork (TM), which is a tissue compartment that was not included in the simplified model]. In the simulation shown in Fig. 5 c for fluorescein, an infinite sink was applied to the boundary for the iris, and a flux condition was applied on the exterior vitreous boundary as specified by Equation 3:

$$\underset{n}{\cdot}(-D\nabla C)=\alpha C \qquad [3]$$

where D is the diffusion coefficient, C is the diffusant concentration, and α is a constant, set to a value of 5×10^{-7} M s^{-1} for this simulation. The value of α depends upon the properties of the diffusing molecule [51].

David Maurice derived the following simple mathematical relationship (Equation 4) for the vitreous elimination rate k_f for materials that are eliminated primarily by the anterior pathway [52]:

$$\frac{C_a}{C_v}=\frac{k_f V_v}{f} \qquad [4]$$

where C_a and C_v are the average concentrations of drug in the aqueous and vitreous compartments respectively, V_v is the volume of the vitreous compartment, and f is the rate of production of aqueous humor. The clearance behavior of several compounds is plotted in Fig. 5 e. The clearance rates for several hydrophilic materials with a range of molecular weights (sucrose, albumin, and dextrans ranging from 10 kDa to 157 kDa) are consistent with the prediction of Equation 4. Fluorescein, which has a molecular weight comparable to that of sucrose, falls far from the curve predicted by the equation, having an approximately tenfold higher rate of clearance from the vitreous and an approximately tenfold lower aqueous concentration. By applying an infinite sink on the iris surface and an imperfect sink on the outer vitreous surface using the expression of Equation 3 with α ranging from 1 $\times 10^{-7}$ M s^{-1} to infinity, the aqueous / vitreous concentration ratio and the vitreal clearance rate fall within the vicinity of the experimental measurement for fluorescein.

Ocular CFD model application: animal to human scaling

When using data collected from dosing a drug in the eyes of animals to predict what would happen if the same drug is administered in human eyes, changes to the anatomy and physiology across species must be taken into account. In simple compartmental models, the changes in geometry between species is frequently reduced to a single parameter, the ratio of the size of the corresponding compartments of the two species to be compared, or the ratio in surface areas of the tissue interface in which drug is eliminated (such as the retina and/or choroid). Similarly, changes in physiology can also be reduced to a single parameter; for example, the difference in the aqueous humor production rate between animals and humans.

Consider the rate of elimination of drug from the anterior chamber. A crude estimate of the rate of clearance might be obtained from the ratio of the rate of aqueous humor refreshment divided by the volume of the anterior chamber. The species dependence of these quantities is provided in Table 3 (Data from

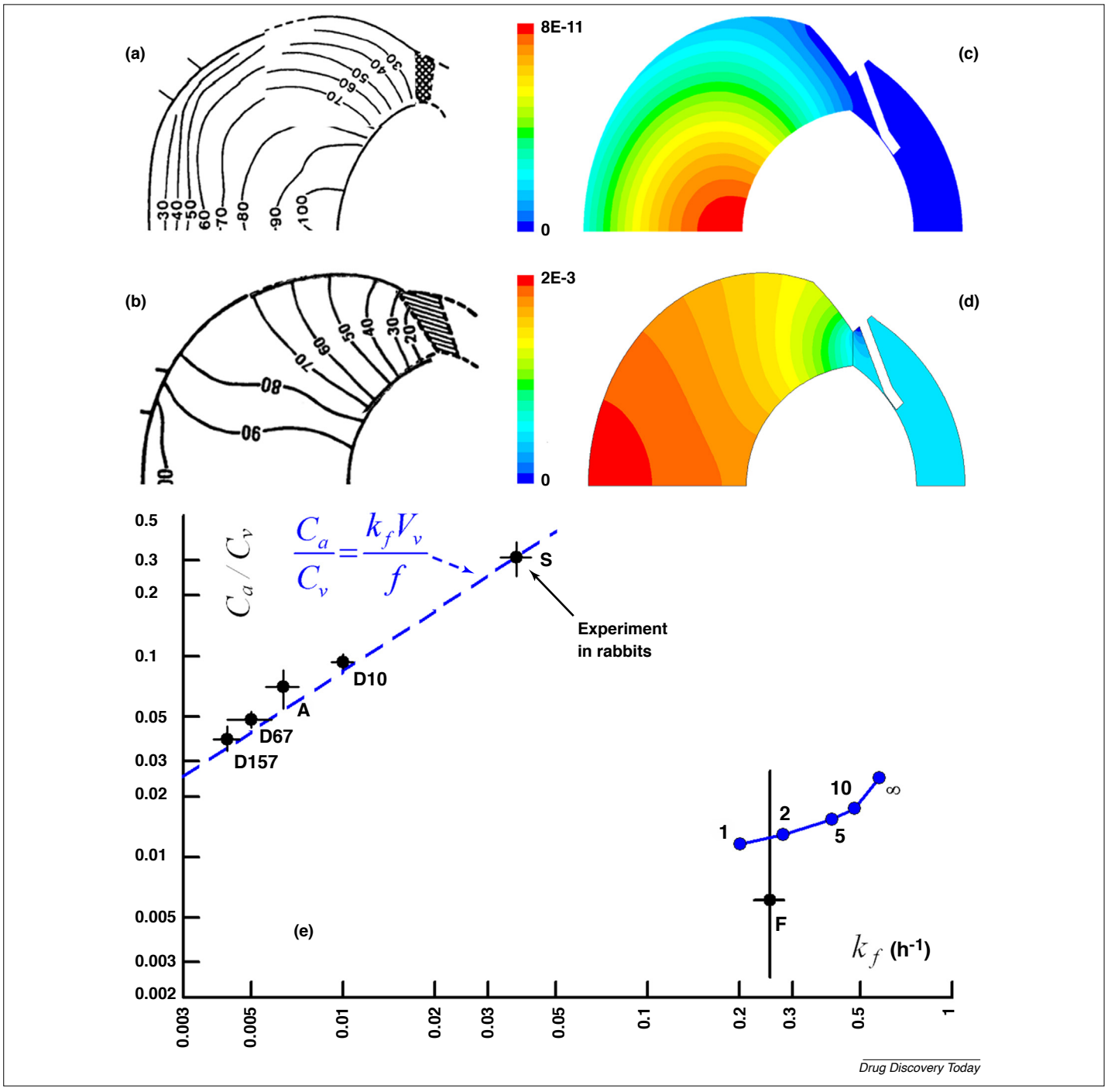

FIGURE 5

Spatial distribution of material after a quasi steady-state has been established for some time following intravitreal (IVT) injection of two materials that are cleared differently from the eye [29]. **(a)** Composite of fluorescent intensity profiles measured from vitreous slices cut from rabbit eyes frozen immediately after euthanasia 15 h after central IVT injection of 15 μl 0.2% fluorescein. **(b)** Similar to (a), but in place of fluorescein, a 0.1% solution of 66 kDa fluorescently labeled dextran had been injected 14 days before euthanasia; in (a,b), 100 refers to the maximum fluorescence intensity. **(c)** Concentration profile predicted 48 h after a simulated central 10 μl bolus injection of fluorescein in the rabbit geometry of [4], vitreous and aqueous compartments only, with an infinite sink applied to the iris surface and the permeability sink of Equation 3 applied at the outer vitreous surface with a value of 5×10^{-7} M s^{-1} for α. **(d)** Concentration profile predicted 48 h after simulated central 10 μl bolus injection of sucrose in the same model, but only allowing injected material to be eliminated by the anterior pathway. In (c,d), the concentration scale is in units of the concentration of material injected. **(e)** Log-log plot of aqueous:vitreous concentration ratio in the terminal elimination phase versus vitreous elimination rate [4]. F, Fluorescein; data from [48]. S, sucrose, data from [49]. D10, D67, and D157, fluorescently labeled dextrans (number in label indicates molecular weight in kDa); data from [40]; A, bovine albumin, data from [50]. Points near F represent simulations of clearance of fluorescein after IVT injection. Each point is labeled with the value of *P* used for the strength of the flux condition applied at the outer vitreous boundary in units of 10^{-7} M s^{-1}.

TABLE 3

Allometric scaling of aqueous humor refreshment for three species

Species	Anterior chamber volume (μl)	Aqueous humor production (μl/min)	Refreshment per h
Rabbit	248[a]	3.0[b]	73%
Monkey	111[a]	1.7[c]	92%
Young human	247[d]	2.8[d]	68%
Older human	160[d]	2.4[d]	90%

[a] Estimated from anatomical models of [4].
[b] From [53].
[c] From [54].
[d] From [55].

[4] and studies [53], [54] and [55] appear in the table.) From Table 3, this ratio in rabbits (73%) would appear to be comparable to the ratio in the eyes of young humans (68%), whereas the ratio in monkeys (92%) is comparable to the ratio in the eyes of older humans (90%). To the extent that drug clearance is influenced by simple fluid turnover, this ratio can be informative, but this simplistic approach ignores the unique manner in which the species-specific anatomy can influence clearance by differences in the structure and placement of interfaces between tissues of other compartments.

The ocular CFD modeling approach can be used to provide an estimate for how drug will distribute following intravitreal injection in one animal species from data obtained in another species as follows. First, model parameters are adjusted to fit the *in vivo* data in the species for which such data are available. Where possible, independent experiments should be conducted to determine physical constants, such as diffusion and partition coefficients (such as in the study of [27]). The strengths of vascular sinks are adjusted to match the clearance rate exhibited by *in vivo* data. Species translation is accomplished by conducting a simulation using the anatomical ocular model for the species of interest, applying all the same parameter values identified in the fit to the first species experiment. Species-specific physiology can be reflected in the unique anatomical structure and/or by adjusting boundary conditions; for example, to apply the appropriate value for fluid inflow on the ciliary body to match the aqueous humor production rate for the particular species. Differences in species are worked out by the differences in physiology, such as compartment volumes, fluid production and/or elimination rates, and intertissue boundaries expressed in the anatomical models. Here, we illustrate this for two similar antibody fragments used to treat macular degeneration: Avastin and Lucentis.

Figure 6 shows a simulation of the time course of drug advection following a hypothetical intravitreal injection of 0.5 mg Lucentis into a human eye. The initial condition was a spherical bolus on the side of the vitreous. Before conducting the advection simulation, the pressure, flow, and temperature of the solution was obtained in the same manner as described earlier. Chemical partitioning was neglected (all partition coefficients set to unity). Drug diffusivity in the vitreous was set to a value of 7.8×10^{-7} cm s^{-2}, an appropriate value for Lucentis in physiological buffer at 37 °C (based on the dynamic light scattering measurements of

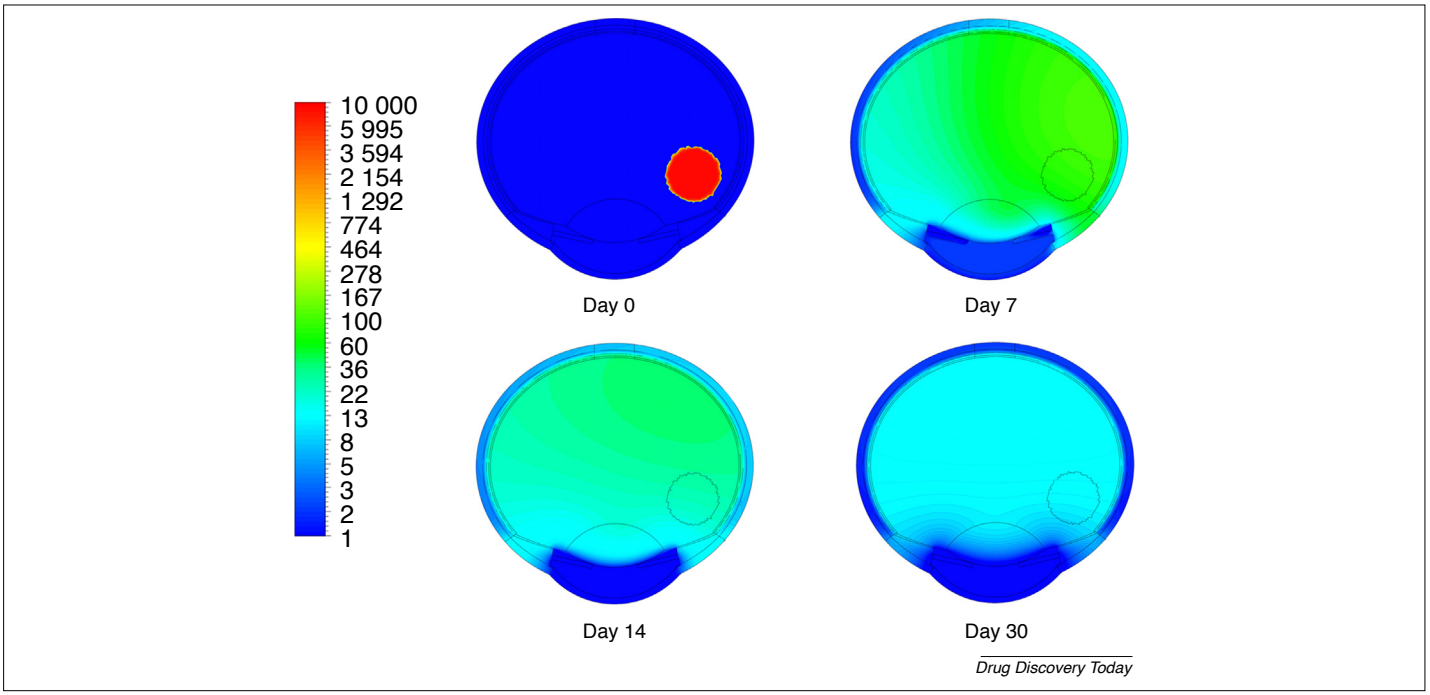

FIGURE 6

Time sequence simulation of advection of 0.5 mg Lucentis after injection in a 50 μl bolus in the position shown on Day 0. Concentration scale in ng/ml.

[56]). Diffusivities in other tissues were scaled according to the following proportions: cornea, sclera, iris, ciliary body, and TM 7.5%; lens 5%; and retina and choroid, 0.75% of the diffusivity assumed for the vitreous (Table 2c). These diffusivity ratios are approximately the same as deduced from tissue transport experiments for a small drug molecule [27]. Regional drug sinks were applied in the ciliary body and the choroid (Table 2d). Note that the sink values for antibody fragments are much lower than those needed for the small drug molecules in Table 1d. Lucentis diffuses more slowly than the small drug molecules considered in the topical dosing simulations described earlier. The drug distribution in the vitreous exhibits asymmetry for several days. Drug can also diffuse through the choroid and into the sclera, and be lost by means of hydraulic efflux through the outer scleral surface. To simulate this efflux effect, the boundary condition of Equation 3 must be modified to include the convective term (Equation 5):

$$\underset{n}{\cdot}\left(-D\nabla C+\overset{C}{v}\right)=\alpha C \qquad [5]$$

Figure 7 illustrates the strategy of species translation using the ocular CFD modeling approach by comparing simulations of mean vitreous and/or aqueous compartment concentrations following IVT injection in rabbits, monkeys, and humans. All simulations were conducted applying the same parameter values of diffusivity and regional sinks, but using the ocular geometry for the appropriate species and setting the flow inlet boundary condition to match the aqueous production rate for each species [4]. The values of the regional sinks were adjusted using the data for clearance after injecting Avastin and Lucentis in the rabbit eye [57,58].

For the animal experiments (Fig. 7 a–c), data are available for both aqueous humor and vitreous compartments. There is a fair match between the simulations and experimental measurements for both aqueous humor and vitreous concentrations in the rabbit for both drugs (Fig. 7 a,b). The simulations correctly predicted the rate of vitreous clearance while simultaneously predicting an appropriate concentration ratio between aqueous humor and vitreous. Note that the sink rates for the antibody fragment drugs (Table 2d) were lower than those used for the small drug molecules considered in the topical dosing simulations (Table 1d); thus, a significant mode of egress for the antibody fragments is via the anterior pathway. This is also reflected by the concentration contour plots of Fig. 5 .

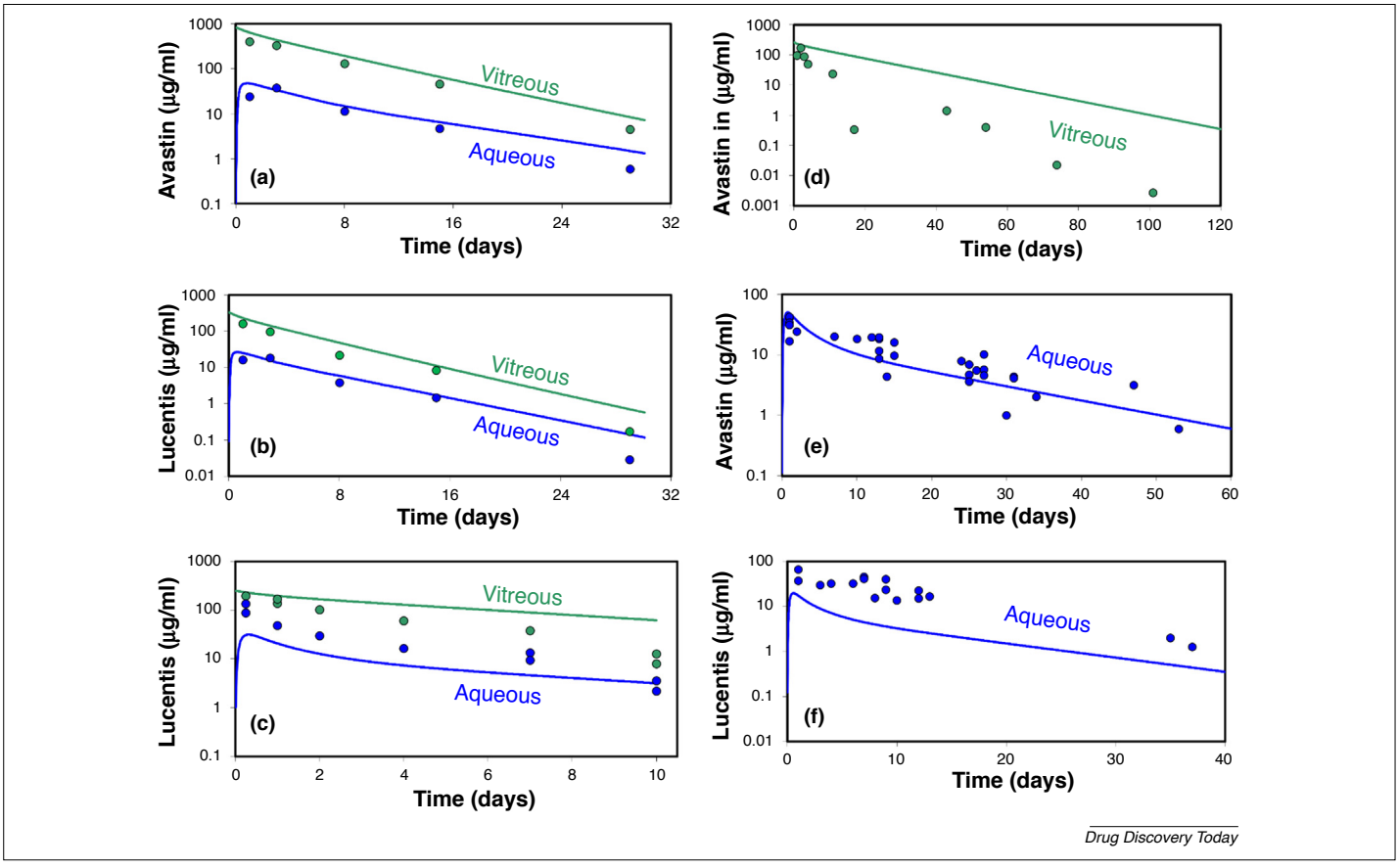

FIGURE 7

Comparison between simulated and experimental pharmacokinetic measurements after intravitreal (IVT) injection in animals [4]. In each case, the initial condition at the beginning of the simulation was a spherical bolus in the mid-vitreous with concentration set as required to administer the amount of drug specified. Solid curves represent the average concentrations in the entire vitreous and aqueous compartments as indicated. **(a)** 1.25 mg Avastin administered in 50 μl to Dutch-belted rabbits [57]. **(b)** 0.5 mg Lucentis administered in 50 μl to Dutch-belted rabbits [58]. **(c)** 0.5 mg Lucentis administered in 50 μl to Cynomolgus monkeys [59]. **(d)** 1.25 mg Avastin administered in 50 μl to patients with submacular hemorrhage and choroidal neovascularization (CNV) resulting from age-related macular degeneration (AMD) [60]. **(e)** 1.25 mg Avastin administered in 100 μl to patients with macular edema secondary to neovascular AMD, diabetic retinopathy, or retinal vein occlusion [61]. **(f)** 0.5 mg Lucentis administered in 100 μl to patients with macular edema secondary to neovascular AMD, diabetic retinopathy, or retinal vein occlusion [62]. Reproduced from [63].

The comparison between simulation and experiment for the monkey [59] (Fig. 7 c) does not show similar agreement. Clearance simulated using the monkey model was slower than the experimental data, and the aqueous humor compartment concentration was underpredicted. For the experiments in humans, data were available for only one compartment. Fig. 7 d shows vitreous Avastin concentration data obtained from patients exhibiting choroidal neovascularization [60]; simulations underpredicted the rate of clearance. Fig. 7 e,f show aqueous humor concentrations of Avastin and Lucentis, respectively, injected into patients with macular edema secondary to neovascular AMD, diabetic retinopathy, or retinal vein occlusion [61,62]. For both of these clinical studies, the simulations appear to predict the correct rate of clearance, although the absolute magnitude was matched only for the Avastin study. The simulations underpredict the magnitude of the aqueous humor concentration for the Lucentis study [63]. The data between the two Krohne *et al.* studies present an interesting phenomenon in that the two data sets appear to superimpose upon each other, despite the fact that the amounts injected differed by more than twofold (1.25 mg Avastin versus. 0.5 mg Lucentis). Either there is a systematic error in one of the analysis sets, or the two drugs, despite their similar properties, behave differently in the eye.

The model appears best qualified for the rabbit eye, and reproduces the clearance rate in humans in the patient populations studied by Krohne *et al.* [61,62]. Drug clears from the monkey eye about as quickly as from the rabbit eye despite the fact that the monkey eye is slightly larger. There might be physiological differences between species that provide an additional means of drug clearance from the vitreous in the monkey. Various investigators have reported on ocular currents that are not captured explicitly in the model [64,65]; some of these might exhibit species differences.

Concluding remarks: applicability to additional drugs and future improvements

The ocular CFD model has the potential for predicting aspects of drug distribution that are not available using traditional compartmental PK models. In addition to modeling the mean concentration within individual tissue compartments, it also can offer insight into how drug is distributed within individual tissue compartments over time. Its application to additional drugs requires knowing their coefficients for diffusion and chemical partitioning into the various tissues of interest. When these are not known, this requires additional *in vitro* experiments to be done to measure these coefficients. In addition, the strengths of the vascular sinks need to be adjusted to fit the data.

The ocular CFD model can be improved and expanded to include the following features, which are beyond the scope of this work: (i) explicit articulation of the anatomy and physiology of the external ocular tissues (lids, conjunctival clearance, and tear-film dynamics); (ii) better understanding of the differences in anatomy and physiology of various species used in ophthalmic studies and incorporation into the species-specific models; (iii) modifications in the model appropriate to account for the effects of age and disease; (iv) alterations in tissue parameters to account for the unique distribution and clearance behavior of different classes of drugs; and (v) application to the development of intraocular sustained drug depots and delivery devices

References

1 Miller, S.C. *et al.* (1981) A physiologically based pharmacokinetic model for the intraocular distribution of pilocarpine in rabbits. *J. Pharm. Biopharm.* 9, 653–677
2 Choudhuri, R.S. *et al.* (2013) Modeling Drug Disposition of Timolol in Ocular Tissues of Rabbit following Topical Eye Drops. *Simulations Plus*
3 Luu, K.T. *et al.* (2009) Pharmacokinetic-pharmacodynamic and response sensitization modeling of the intraocular pressure-lowering effect of the EP4 agonist 5-{3-[(2S)-2-{(3R)-3-hydroxy-4-[3-(trifluoromethyl)phenyl]butyl}-5-oxopyrrolidin-1-yl]propyl}thiophene-2-carboxylate (PF-04475270). *J. Ocular Pharm. Ther.* 331, 627–635
4 Missel, P.J. (2012) Simulating intravitreal injections in anatomically accurate models for rabbit, monkey and human eyes. *Pharm. Res.* 29, 3251–3272
5 Heys, J.J. and Barocas, V.H. (2002) A Boussinesq model of natural convection in the human eye and the formation of Krukenberg's spindle. *Ann. Biomed. Eng.* 30, 392–401
6 Kumar, S. *et al.* (2007) Deposition of particles on ocular tissues and formation of Krukenberg spindle, hyphema, and hypopyon. *J. Biomech. Eng.* 129, 174–186
7 Heys, J.J. and Barocas, V.H. (2002) Computational evaluation of the role of accommodation in pigmentary glaucoma. *Invest. Ophthalmol. Vis. Sci.* 43, 700–708
8 Amini, R. *et al.* (2012) Increased iris-lens contact following spontaneous blinking: Mathematical modeling. *J. Biomech.* 45, 2293–2296
9 Keister, J.C. *et al.* (1991) Limits on optimizing ocular drug delivery. *J. Pharm. Sci.* 80, 50–53
10 Chrai, S.S. *et al.* (1973) Lacrimal and instilled fluid dynamics in rabbit eyes. *J. Pharm. Sci.* 62, 1112–1121
11 Ahmed, I. *et al.* (1987) Physicochemical determinants of drug diffusion across the conjunctiva, sclera, and cornea. *J. Pharm. Sci.* 76, 583–586
12 Higashiyama, M. *et al.* (2004) Improvement of the ocular bioavailability of timolol by sorbic acid. *Int. J. Pharm.* 272, 91–98
13 Ohtori, A. and Tojo, K. (1994) *In vivo* / *in vitro* correlation of intravitreal delivery of drugs with the help of computer simulation. *Biol. Pharm. Bull* 17, 283–290
14 (1996) Finite element modeling of drug distribution in the vitreous humour of the human eye. In *Annual Meeting of the Association for Research in Vision and Ophthalmology*. Poster, Fort Lauderdale
15 Friedrich, S. *et al.* (1997) Finite element modeling of drug distribution in the vitreous humor of the rabbit eye. *Ann. Biomed. Eng.* 25, 303–314
16 Stay, M.S. *et al.* (2003) Computer simulation of convective and diffusive transport of controlled-release drugs in the vitreous humor. *Pharm. Res* 20, 96–102
17 Park, J. *et al.* (2005) Evaluation of coupled convective–diffusive transport of drugs administered by intravitreal injection and controlled release implant. *J. Control. Release* 105, 279–295
18 Balachandran, R.K. and Barocas, V.H. (2008) Computer modeling of drug delivery to the posterior eye: effect of active transport and loss to choroidal blood flow. *Pharm. Res.* 25, 2685–2696
19 Balachandran, R.K. and Barocas, V.H. (2011) Contribution of saccadic motion to intravitreal drug transport: theoretical analysis. *Pharm. Res.* 28, 1049–1064
20 Missel, P.J. (2000) Finite element modeling of diffusion and partitioning in biological systems: the infinite composite medium problem. *Ann. Biomed. Eng.* 28, 1307–1317
21 Missel, P.J. (2002) Finite and infinitesimal representations of the vasculature: ocular drug clearance by vascular and hydraulic effects. *Ann. Biomed. Eng.* 30, 1128–1139
22 Missel, P.J. (2002) Hydraulic flow and vascular clearance influences on intravitreal drug delivery. *Pharm. Res* 19, 1636–1647
23 Missel, P.J. *et al.* (2003) *Predicting Ocular Drug Levels from Intravitreal Administration of Anecortave Acetate (AL-3789).* Poster; Annual Meeting of the Biomedical Engineering Society, Nashville
24 Missel, P. *et al.* (2006) A clear vision for drug delivery. *Fluent News* 15, s8–s10
25 Missel, P. (2009) *Computer modeling of Pharmacokinetics from Ocular Drug Delivery.* . Lecture; Association for Research in Vision and Ophthalmology Summer Eye Research Conference on Ophthalmic Drug Delivery Systems for the Treatment of Retinal Diseases: Basic Research to Clinical Application, Bethesda

26 Missel, P.J. *et al.* (2010) Dissolution of intravitreal Triamcinolone Acetonide suspensions in an anatomically accurate rabbit eye model. *Pharm. Res.* 27, 1530–1546

27 Missel, P. *et al.* (2010) *In vitro* transport and partitioning of AL-4940, active metabolite of angiostatic agent Anecortave Acetate, in ocular tissues of the posterior segment. *J. Ocular Pharmacol. Ther.* 26, 137–145

28 Lamminsalo, M. *et al.* (2018) Extended pharmacokinetic model of the rabbit eye for intravitreal and intracameral injections of macromolecules: quantitative analysis of anterior and posterior elimination pathways. *Pharm. Res.* 35, 153

29 Missel, P.J. (2013) Computer modeling for ocular drug delivery. In *Ocular Drug Delivery, Systems, Applications of Nanoparticulate Systems* (Thassu, D. and Deleers, M., eds), pp. 59–98, CRC Press

30 Schoenwald, R.D. (1985) The control of drug bioavailability from ophthalmic dosage forms. In *Controlled Drug Bioavailability* (Smolen, V.F. and Ball, L.A., eds), pp. 257–306, Wiley

31 Owen, G.R. *et al.* (2007) A novel *in vivo* rabbit model that mimics human dosing to determine the distribution of antibiotics in ocular tissues. *J. Ocular Pharm. Ther.* 23, 335–342

32 Robertson, S.M. *et al.* (2005) Ocular pharmacokinetics of Moxifloxacin after topical treatment of animals and humans. *Surv. Ophthalmol.* 50, S32–S45

33 Francoeur, M.L. *et al.* (1985) Kinetic disposition and distribution of timolol in the rabbit eye. A physiologically based ocular model. *Int. J. Pharm.* 25, 275–292

34 Missel, P.J. and Horne, M. (2015) Modeling ocular drug delivery using computational fluid dynamics. *OnDrugDelivery* 54, 12–16

35 Zhang, Y. *et al.* (2018) Three-dimensional transport model for intravitreal and suprachoroidal drug injection. *Invest. Ophthalmol. Vis. Sci.* 59, 5266–5276

36 Jooybar, E. *et al.* (2014) Computational modeling of drug distribution in the posterior segment of the eye: Effects of device variables and positions. *Math. Biosci.* 255, 11–20

37 Kotliar, K. *et al.* (2007) Effect of intravitreal injections and volume changes on intraocular pressure: clinical results and biomechanical model. *Acta Ophthalmol. Scand.* 85, 777–781

38 Maurice, D.M. (1987) Flow of water between aqueous and vitreous compartments of the rabbit eye. *Am. J. Physiol.* 252, F104–F108

39 Molokhia, S.A. *et al.* (2009) Transscleral iontophoretic and intravitreal delivery of a macromolecule: study of ocular distribution *in vivo* and postmortem with MRI. *Exp. Eye Res.* 88, 418–425

40 Johnson, F. and Maurice, D. (1984) A simple method of measuring aqueous humor flow with intravitreal fluoresceinated dextrans. *Exp. Eye Res.* 39, 791–805

41 Lee, B. *et al.* (1992) Rheology of the vitreous body, part I: viscoelasticity of the human vitreous. *BioRheology* 29, 521–533

42 Lee, B. *et al.* (1994) Rheology of the vitreous body, part II: viscoelasticity of bovine and porcine vitreous. *BioRheology* 31, 327–338

43 Sebag, J. (1987) Age-related changes in human vitreous structure. *Graefe's Arch. Clin. Exp. Ophthalmol.* 225, 89–93

44 Beer, P.M. *et al.* (2003) Intraocular concentration and pharmacokinetics of Triamcinolone Acetonide after a single intravitreal injection. *Ophthalmology* 110, 681–686

45 Lee, S.S. *et al.* (2010) Vitreous VEGF clearance is increased after vitrectomy. *Invest. Ophthalmol. Vis. Sci.* 51, 2135–2138

46 Chang-Lin, J.-E. *et al.* (2011) Pharmacokinetics of a sustained-release dexamethasone intravitreal implant in vitrectomized and nonvitrectomized eyes. *Invest. Ophthalmol. Vis. Sci.* 52, 4605–4609

47 Araie, M. and Maurice, D.M. (1991) The loss of fluorescein, fluorescein glucuronide and fluorescein isothiocyanate dextran from the vitreous by the anterior and retinal pathways. *Exp. Eye Res.* 52, 27–39

48 Cunha-Vaz, J. and Maurice, D. (1969) Fluorescein dynamics in the eye. *Doc. Ophthalmol* 26, 61–72

49 Bito, L.Z. and Salvador, E.V. (1972) Intraocular fluid dynamics III. The site and mechanism of prostaglandin transfer across the blood intraocular fluid barriers. *Exp. Eye Res.* 14, 233–241

50 Maurice, D.M. (1959) Protein dynamics in the eye studied with labelled proteins. *Am. J. Ophthalmol.* 47, 361–367

51 Haghjou, N. *et al.* (2013) Retina-choroid-sclera permeability for ophthalmic drugs in the vitreous to blood direction: quantitative assessment. *Pharm. Res.* 30, 41–59

52 Maurice, D.M. (1976) Injection of drugs into the vitreous body. In *Symposium on Ocular Therapy* (Leopold, T. and Burns, R., eds), pp. 59–72, Wiley

53 Reitsamer, H.A. *et al.* (2009) Effects of Dorzolamide on choroidal blood flow, ciliary blood flow, and aqueous production in rabbits. *Invest. Ophthalmol. Vis. Sci.* 50, 2301–2307

54 Rasmussen, C.A. *et al.* (2007) Aqueous humor dynamics in monkeys in response to the kappa opioid agonist bremazocine. *Trans. Am. Ophthalmol. Soc.* 105, 225–239

55 Toris, C.B. *et al.* (1999) Aqueous humor dynamics in the aging human eye. *Am. J. Ophthalmol.* 127, 407–412

56 Wen, H. *et al.* (2013) Characterization of human sclera barrier properties for transscleral delivery of Bevacizumab and Ranibizumab. *J. Pharm. Sci.* 102, 892–903

57 Bakri, S.J. *et al.* (2007) Pharmacokinetics of intravitreal Bevacizumab (Avastin). *Ophthalmology* 114, 855–859

58 Bakri, S.J. *et al.* (2007) Pharmacokinetics of intravitreal Ranibizumab (Lucentis). *Ophthalmology* 114, 2179–2182

59 Gaudreault, J. *et al.* (2005) Preclinical pharmacokinetics of Ranibizumab (rhuFabV2) after a single intravitreal administration. *Invest. Ophthalmol. Vis. Sci.* 46, 726–733

60 Zhu, Q. *et al.* (2008) Vascular Endothelial Growth Factor-A in patients with choroidal neovascularization. *Ophthalmology* 115, 1750–1755

61 Krohne, T.U. *et al.* (2008) Intraocular pharmacokinetics of Bevacizumab after a single intravitreal injection in humans. *Am. J. Ophthalmol.* 146, 508–512

62 Krohne, T.U. *et al.* (2012) Intraocular pharmacokinetics of Ranibizumab following a single intravitreal injection in humans. *Am. J. Ophthalmol.* 154, 682–686

63 Missel, P.J. (2013) *Qualification of Ocular CFD Models to Aid Development of Intravitreal Anti-VEGF Therapies*. Poster, ACOP, Fort Lauderdale

[64] Hayreh, S.S. (1966) Posterior drainage of the intraocular fluid from the vitreous. *Exp, Eye Res.* 5, 123–144

65 Fowlks, W.L. and Havener, V.R. (1964) Aqueous flow into the perivascular space of the rabbit ciliary body. *Invest. Ophthalmol.* 3, 374–383